Quaternary Geochronology 67 (2022) 101237

Contents lists available at ScienceDirect

Quaternary Geochronology

journal homepage: www.elsevier.com/locate/quageo

New chronological constraints on the Plio-Pleistocene uplift of the Guizhou Plateau, SE margin of the Tibetan Plateau

Yu Liu [a,b], Shijie Wang [a,b], Sheng Xu [c], Derek Fabel [d], Finlay M. Stuart [d], Ángel Rodés [d], Xinbao Zhang [e], Weijun Luo [a,b,*]

[a] State Key Laboratory of Environmental Geochemistry, Institute of Geochemistry, Chinese Academy of Sciences, Guiyang, 550081, China
[b] Puding Karst Ecosystem Research Station, Chinese Academy of Sciences, Puding, 562100, China
[c] Institute of Surface-Earth System Science, Tianjin University, Tianjin, 300072, China
[d] Scottish Universities Environmental Research Centre, East Kilbride, G75 0QF, United Kingdom
[e] Institute of Mountain Hazards and Environment, Chinese Academy of Sciences, Chengdu, 610041, China

ARTICLE INFO

Keywords:
Cosmogenic isotopes
Burial dating
Cave sediments
Fluvial terraces
Guizhou plateau
China

ABSTRACT

The Guizhou Plateau represents a geomorphic transition between the Tibetan Plateau and the Yangtze River Plain. It likely formed in response to the propagation of surface uplift in southeastern Tibet during India-Eurasia continental collision. However, the uplift history of the region is unclear largely due to a lack of datable material. The bedrock geology is dominated by carbonate rocks, which contains numerous multi-level caves in the main river valleys that are linked to the river incision history. Cosmogenic ^{26}Al and ^{10}Be burial dating of sediments in caves and river terraces from the northwestern and southern plateau reveals the fluvial chronology and provides the first direct determination of long-term river incision rates. The caves and terraces on the Liuchong River in NW Guizhou yield burial ages of between 0.41 ± 0.12 Ma and 2.85 ± 0.21 Ma, indicating an average incision rate of 57 ± 3 m/Ma. Four level caves at Libo in southern Guizhou yield burial ages of between 0.56 ± 0.16 Ma and 3.54 (+0.25/-0.22) Ma, indicating slightly slower incision rate (47 ± 5 m/Ma). These new results imply that the high elevation of the Guizhou Plateau had developed before the Late Pliocene, and that surface uplift during the Late Cenozoic was largely uniform across the region.

1. Introduction

The Tibetan Plateau is the most extensive area of elevated topography in the world. Studies of the inter-relationship between tectonics and climate provide the key to determining the timing and mechanism of plateau uplift in the Cenozoic (e.g. Molnar and Tapponnier, 1975; Molnar et al., 1993; Clark et al., 2004; An et al., 2011). Studies have mostly focused on the plateau interior and several plateau margins (e.g. Clark et al., 2005; Hetzel et al., 2006; Schoenbohm et al., 2006; Wang et al., 2008; Henck et al., 2011; Li et al., 2014). In comparison to the topographically steep margins of the Himalayas, the Kunlun Mountains and Longmen Shan, the topographic gradient (and the crustal thickness) along the southeastern margin of the Tibetan Plateau is more subdued, steadily decreasing from Tibet to the continental margin in response to crustal deformation with continental extrusion (Clark and Royden, 2000; Wang et al., 2003). This region is known as the Yunnan-Guizhou Plateau (or abbreviated as the Yungui Plateau; Fig. 1a). Studies of the topographic growth mechanism and plateau uplift history have primarily focused on constraining the western part of the Yungui Plateau, termed the Yunnan Plateau. One widely held model (Clark and Royden, 2000) suggests that lower crustal flow from beneath Tibet into adjacent regions was blocked by mechanically strong lithosphere (e.g., the Sichuan Basin), which led to the development of a steep topographic margin (such as the Longmen Shan) while unimpeded flow caused a southeastward propagation of surface uplift (Schoenbohm et al., 2006). This hypothesis remains disputed. Several geophysical studies indicate that unhindered crustal flow beneath SE Tibet may not occur (e.g. Sol et al., 2007; Yao et al., 2008), while thermochronology of the eastern Tibet and 2008 Wenchuan earthquake imply that crustal shortening is the primary driver of uplift (Hubbard and Shaw, 2009; Wang et al., 2012). Recent paleoaltimetric studies based on stable isotopes suggest that the near present-day high elevation of the SE Tibetan Plateau (Yunnan) existed in the Eocene (Hoke et al., 2014; Li et al., 2015; Wu et al., 2018). In contrast, low-temperature thermochronology suggest

* Corresponding author. 99 Lincheng West Road, Institute of Geochemistry, Chinese Academy of Sciences, Guiyang, 550081, China.
E-mail address: luoweijun@mail.gyig.ac.cn (W. Luo).

https://doi.org/10.1016/j.quageo.2021.101237
Received 12 October 2020; Received in revised form 3 September 2021; Accepted 28 September 2021
Available online 30 September 2021

that widespread crustal shortening and thickening in SE Tibet initiated at 20–28 Ma, with rapid increase in mean elevation beginning at 13–15 Ma followed by a stepwise accelerated rise at ~5 Ma, ~3.5 Ma, ~1.8 Ma and ~1.0 Ma (Clark et al., 2005; Lei et al., 2008; Cao et al., 2019). This conclusion is supported by sedimentation rates and sediment fluxes in the South China Sea (Wang et al., 2000; Clift and Sun, 2006).

The Guizhou Plateau forms the eastern part of the Yungui Plateau. It is a large mountainous karst region with rugged terrain that includes steep karst peaks and deep gorges (Fig. 1) and marks the transition between the Yungui Plateau and the South China Plain. The poor Cenozoic sediment record on the predominantly karst landscape has restricted research on the uplift history. Paleogeographic evidence implies that the eastern part of Guizhou was topographically higher than the western region before the Neogene (Lin, 1993). A widespread erosion surface developed during the Tertiary and Early Quaternary (Yang, 1944). From the middle Pleistocene to the present, large scale east-tilted uplift driven by the uplift of the Tibetan Plateau generated the modern topography (GBGMR, 1987; Lin, 1993). Geomorphology and the sediment record indicate that 1–2 km of surface uplift occurred in the west-central part of the Guizhou Plateau during the Quaternary, and several hundred meters of uplift occurred in the eastern part (Lin, 1993). This is based on the existence of vestiges of an ancient planar surface which formed a contiguous surface graded to the marine base level and is now at 2.0–2.3 km above sea level in the west and 0.7–0.8 km in the east (GBGMR, 1987; Lin, 1993; Lin et al., 1994; Zhou et al., 2005). Apatite fission track-derived cooling ages shows that central Guizhou has experienced ~2.8 km of rock uplift in the last 70 Ma, with ~1.1 km uplift in the last 5 Ma (Luo et al., 2009).

Fluvial terraces and caves in the region record the progressive vertical fluvial aggradation/incision of river valleys caused by tectonic uplift and/or climate oscillations (Zhou et al., 2005; Kong et al., 2010). Uneroded fluvial terraces of the main rivers at high elevations are scarce. Absolute age constraints on terrace formation have been difficult to obtain, and previous studies have dated terraces with relative age techniques that do not allow for robust determination of formation time and thus incision rates (Kong et al., 2010). Cave systems are widely distributed in the river canyons of Guizhou. U-series dates put the formation of the oldest speleothem in the cave at before 350 ka (Yang, 1998). *In-situ* cosmogenic nuclide dating is a reliable method for determining the time of cave development in mountainous regions (Partriage et al., 2003; Stock et al., 2005). We previously used cosmogenic $^{26}Al/^{10}Be$ burial dating of quartz-rich sediments from the Liuchong River in NW Guizhou to determine the incision history of the major drainage system of the Guizhou Plateau (Liu et al., 2013a). However, the data could not be used to establish a robust incision history as the burial ages were inconsistent with a simple chronological sequence.

In order to obtain a better understanding of the incision history of the Liuchong River and the propagation of Guizhou Plateau uplift we report a new study of cosmogenic nuclide burial ages of caves and terraces preserved along the Liuchong River (northwestern Guizhou) and Libo County (southern Guizhou). This has allowed the late Cenozoic fluvial chronology and valley incision rates to be determined.

2. Study areas and sample analysis

2.1. Regional setting

The Guizhou Plateau is an east-tilted upland region bounded in the west by the Wumeng Shan and by lowland regions to the north, east and

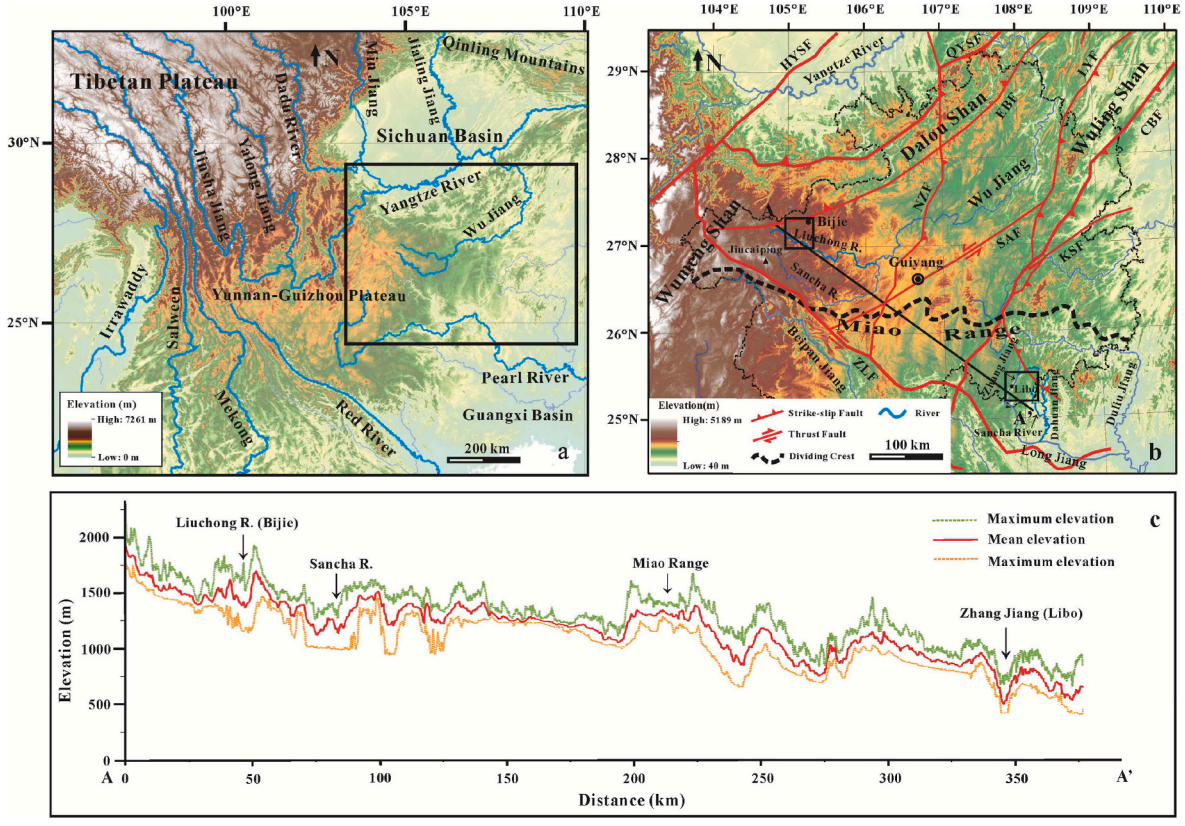

Fig. 1. Map showing the geographical position of the study area. (a) Location of the Guizhou Plateau in the southeastern Tibetan Plateau. (b) Digital Elevation Model (DEM) of the Guizhou Plateau. The black box indicates the location of study areas shown in Fig. 2. CBF=Cili-Baojing Fault; EBF = Enshi-Bijie Fault; HYSF=Huayingshan Fault; KSF=Kaili-Sandu Fault; LYF = Laifeng-Yinjiang Fault; NZF=Nanchuan-Zunyi Fault; QYSF = Qiyueshan Fault; SAF=Shiqian-Anshun Fault; ZLF = Ziyun-Luodian Fault. (c) Topography along A-A′ as determined by swath profiles showing systematic decrease in mean altitude along the northwestern and southern Guizhou Plateau.

south (Fig. 1b). The Dalou Shan runs along the boundary with the Sichuan Basin in the north, and the Wuling Shan in the northeast forms a barrier between the Guizhou Plateau and the Yangtze Plain. In the south, the Miao Range steps down to the karst hills of the Guangxi Basin, and represents the watershed of the Yangtze River and the Pearl River (Fig. 1b). Rivers starting on the north side of the Miao Range flow into the Yangtze River catchment, and the rivers on the south slope flow into the Pearl River. The mean altitude of the Guizhou Plateau is approximately 1100 m, and the highest peak Jiucaiping in the west, has an altitude of 2900 m (Fig. 1b). The regional bedrock is dominantly carbonate rocks that formed from the Late Sinian to middle Late Triassic. The Indosinian orogeny at the end of the Late Triassic led to surface uplift and deposition of terrestrial lacustrine sediments. The Early Cretaceous Yanshanian orogeny led to crustal deformation and the formation of the modern tectonic and landscape setting of the plateau (GBGMR, 1987).

The Guizhou Plateau is not considered to be an active orogenic plateau, unlike the adjacent Yunnan Plateau. Seismicity is negligible, and vertical elevation changes are the primary evidence of neo-tectonic movement (GBGMR, 1987). A series of staircase landforms have developed that are characterized by multilevel planation surfaces, fluvial terraces and caves that record the episodic uplift of Guizhou (Lin, 1993; Lin et al., 1994; Zhou et al., 2005). Using the elevation and geomorphology of the main mountains Yang (1944) proposed three evolutionary stages, the Daloushan (Paleogene), Shanpen (Neogene) and Wujiang (Quaternary) stages. The first two stages represent relatively stable tectonic periods, while the last stage is characterised by active erosion and the intensive incision of the Wu Jiang river. The Guizhou landscape is considered to have formed in the early Pleistocene (Lin, 1993), evidenced by the absence of lower Pleistocene sediments (Lin et al., 1994). From the end of the Lower Pleistocene to the Holocene the region experienced episodic river incision that formed caves and fluvial terraces in the river valleys and is regarded as the time the modern landscape formed (Lin et al., 1994).

2.2. Site description and sample collection

2.2.1. The Liuchong River in NW Guizhou

The Liuchong River is situated in the transition zone between the eastern Yunnan Plateau and the central Guizhou Plateau. The average altitude declines from 2000 m to 1000 m (Fig. 1b). It is a northern tributary of the Wu Jiang, the largest river in Guizhou, and flows across the northwestern Guizhou Plateau. It cuts 300–400 m into the Triassic carbonate rocks and has produced seven cave levels (A to G) in the river canyon wall in the Bijie area (Fig. 2a–c). In this study six of the seven cave levels from a ~35 km long section of the Liuchong River between Qixingguan and Jiayan village have been sampled and dated (Fig. 2b and c). The caves display rather simple horizontal networks that they were the past drainage outlets of the main rivers. The river surface altitude of the Liuchong River in this region is approximately 1200 m.

Xiao Cave (XC) is the highest cave currently found in the main stem canyon. It is present on the south bank at 1550 m above sea level (a.s.l.), 350 m above the modern river level (AML; level A). It is a large cave (>100 m long, 20 m wide and 15 m high) and contains a 5 m thick fluvial deposit. No quartz was found in the deposit. Shenxian Cave (SXC, 1420 m a.s.l.) at Qixingguan and Wangtian Cave (WTC, 1432 m a.s.l.) at Jiayan represent level B in the study area (220–230 m AML). SXC was previously yielded a $^{26}Al/^{10}Be$ burial age of 1.46 (+1.32/-0.80) Ma, the large uncertainty reflecting the extremely low ^{10}Be and ^{26}Al concentrations (Liu et al., 2013a). The lower Dayan Cave (DYC) of level C (145 m AML) located near Jiayan, yielded a $^{26}Al/^{10}Be$ burial age of 2.85 ± 0.21 Ma from amalgamated pebbles (Liu et al., 2013a) that is older than that in SXC (albeit within analytical uncertainty). Shanshu Cave (SSC) is approximately 2.5 km west of Jiayan, at ~80 m AML and corresponds to the fourth regional level (level D). Dashi Cave (DSC, 1512 m a.s.l.) and Yantougou Cave (YTGC, 1530 m a.s.l.) at 50–60 m AML mark level E. DSC and YTGC are located in two tributary canyons of the Liuchong River, the Bizhi River and the Touwan River, respectively (Fig. 2b). DSC yielded a lower pebble burial age of 0.75 ± 0.10 Ma and an upper sand burial age of 0.69 ± 0.10 Ma, while YTGC yielded a burial age of 0.49 ± 0.13 Ma (Liu et al., 2013a). These two ages overlap within uncertainty suggesting that level E was formed at 0.49–0.75 Ma. Chushui Cave (CSC) is ~30 m AML marks the level F in this area. These caves are hydrologically abandoned and are above the modern flood zone. The cave passages at 5–10 m AML (level G), e.g. Guanyin Cave (GYC) under the Qixingguan Bridge, are within the modern flood zone and may correspond to small, discontinuous terraces above the modern floodplain. No suitable samples were found in level F and G caves, so we sampled the nearby strath terraces that are equivalent to the two levels (Terrace 2 and Terrace 1) at Pingzi village and Houchang village (Fig. 2b). Terrace 2 (T2) is a 2–3 m thick section of the gravels overlying the yellow mudstone bedrock that is ~15 m AML and represents cave level F. Terrace 1 (T1) is equivalent to level G, it is 2 m thick and 5–10 m AML. In order to assess incomplete shielding the two terraces were dated by the isochron burial method. Five individual cobbles from a horizontal layer at the bottom of each terrace deposits were collected. In addition, a sand sample from DYC and a sample of amalgamated pebbles from SSC were collected for burial dating.

2.2.2. Libo in southern Guizhou

Libo County is situated in the transition zone between the Guizhou Plateau and the Guangxi Basin. The mean elevation declines from 1000 m to less than 200 m (Fig. 1b and c). The Di'e River, Zhang Jiang and Sancha River are the three primary rivers (Fig. 2e). The Zhang Jiang is the largest regional river, with the Di'e River merging into the Zhang Jiang at Wangmeng (Fig. 2e). The Sancha River is a tributary of the Dahuan Jiang. They flow south into the Long Jiang, a tributary of the Pearl River in the northern Guangxi Basin (Fig. 1b). The regional geology is dominated by Carboniferous carbonate rocks (Fig. 2d) and is part of the South China Karst, a UNESCO World Heritage Site since 2007. Four cave levels were previously identified: The caves at 800–900 m a.s.l. mark the uppermost cave passages while those at 650–700 m a.s.l. and 520–580 m a.s.l. are large (usually 10 m high, 30–50 m wide and more than 200 m in length) and represent the most stable regional cave formation period. The cave passages below 500 m are the modern hydrologically-active water passages. Based on cave morphology, sediment type and elevation distribution, these caves were formed in the Cretaceous, Tertiary, Lower Pleistocene and Upper Pleistocene, respectively (Zhang et al., 2000).

In this study, six cave levels have been identified in the river canyons at Libo. Here the river surface altitude of the Zhang Jiang is approximately 425 m. The two highest caves, Ganya Cave (GYC, 880 m a.s.l.) and Bieduo Cave (BDC, 785 m a.s.l.) are 455 m and 360 m above the modern Zhang Jiang respectively, and represent the uppermost (level A′) and second highest cave (level B′) levels in this area. No samples were found in these two caves due to collapses. Yamen Cave (YMC) is situated near the main valley of the Zhang Jiang, 12 km northeast of Libo town (Fig. 2e). YMC is 587 m a.s.l. (162 m AML), representing level C′ of this region. The other four cave levels (levels C′ to F′) are found in the Maolan River valley. The Maolan River is a tributary of the Sancha River to the west and turns into an underground river at the end of the valley (Fig. 2e). The river merges into the Sancha River at Wuyan Bridge (Fig. 2e). The current water surface of the Maolan River in the blind valley is 565 m. Jiudongtian Cave (JDTC) is a pass-through cave with an elevation of 715 m a.s.l. (150 m AML) and is at a similar elevation above the main river as YMC, which is on level C'. The speleothems are well developed and no sediment was found for burial dating. Dongge Cave (DGC) is a multi-level cave system that contains three floors and has been used extensively for paleoclimate research (e.g. Yuan et al., 2004). The first cave level is at 680–690 m, the second level is at 620–650 m, and the lowest level is at 560–580 m. A sample was collected at the second cave level at ~650 m a.s.l.. The DGC sample is ~85 m AML and

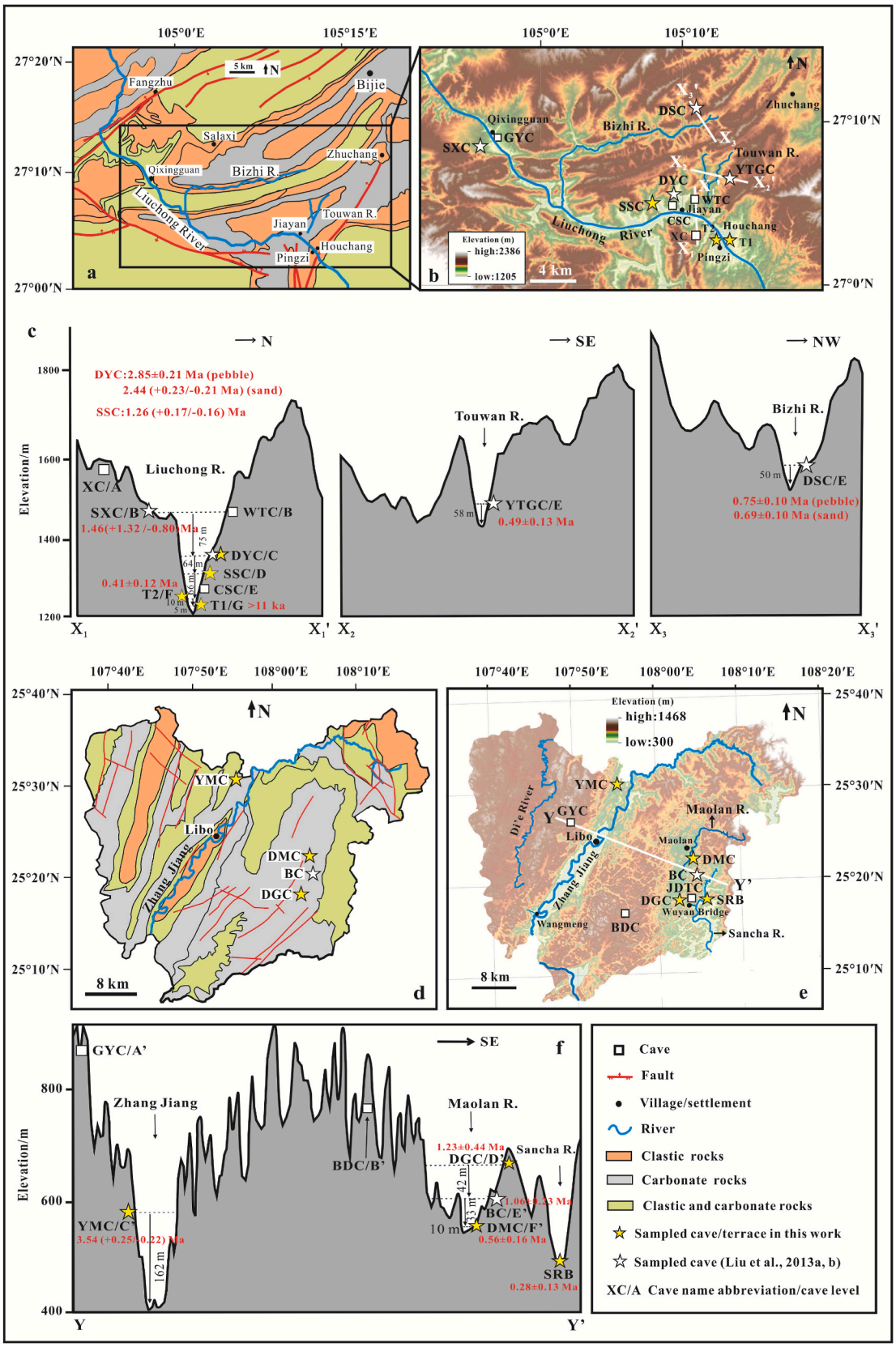

Fig. 2. (a) Simplified geological map of the Liuchong River region near Bijie. (b) Sampled cave localities along the Liuchong River valley marked with stars. (c) Sketch map of cave system of the Liuchong River. (d) Simplified geological map of the Libo County. Sampled cave localities are marked with stars. (e) DEM picture of the Libo County. (f) Sketch map of cave systems in Libo. Labeling of sample acronyms as used in Table 1.

thus corresponds to regional level D'. Black Cave (BC) is 43 m AML at 608 m a.s.l. and represents level E'. BC is close to DGC and yielded a $^{26}Al/^{10}Be$ burial age of 1.06 ± 0.23 Ma (Liu et al., 2013b). Dongmen Cave (DMC, level F') is a pass-through cave at 575 m and is approximately 10 m above the modern Maolan River.

Three samples of amalgamated pebbles from YMC, DGC and DMC were collected for burial dating. A surface sample collected from the modern bank of the Sancha River (SRB; 480 m a.s.l.; Fig. 2e) was used to test for the presence of inherited cosmogenic nuclides in the cave samples.

Detailed information about the location and morphology of each sampled cave and terrace is provided in Table 1. Pictures of the sampled caves and terraces from the two study areas are shown in Figs. 3 and 4. At least 1 kg of quartz-rich pebbles or sand was collected at each site. The cave samples were buried more than 20 m. The caves have morphologies that clearly link them to former river positions and they formed downstream of any established glacial limits, where canyon downcutting was accomplished solely by river incision processes or in response to long-term tectonic uplift.

2.3. Sample preparation and analysis

Quartz was separated and purified in the State Key Laboratory of Environmental Geochemistry, Institute of Geochemistry, Chinese Academy of Sciences. One cobble sample from T1 on the Liuchong River weighed less than 10 g after chemical purification and was not used. Beryllium and aluminum extraction and purification, accelerator mass spectrometry (AMS) measurement of 26Al and 10Be concentration, and total Al determination by inductively coupled plasma optical emission spectrometry (ICP-OES; PerkinElmer, Optima 5300DV, assigned 3% uncertainty) were all performed at the Scottish Universities Environmental Research Centre (SUERC). The 0.125–0.25 mm size fraction was used for quartz purification by selective chemical dissolution (Kohl and Nishiizumi, 1992). The purified quartz (~20 g) was dissolved in a solution of concentrated HF and HNO3. Approximately 0.2 mg Be carrier was added to the samples and blanks. Al carrier (~1.5 mg) was spiked only in the blanks due to the 27Al concentration of samples. Al and Be were extracted and separated by ion chromatography and selectively precipitated as hydroxides. The precipitates were oxidized at 800 °C. The Al2O3 and BeO were mixed with Ag and Nb matrix respectively and then pressed into a Cu sample holder for AMS analysis (Xu et al., 2015). Procedural blanks processed in association with the samples have a mean 10Be/9Be of 3.59 × 10–15 and 26Al/27Al of 6.18 × 10–16. Measured 26Al/27Al and 10Be/9Be ratios are normalized to primary standards Z92-0222 with a nominal 26Al/27Al of 4.11 × 10–11 and NIST SRM 4325 with a nominal 10Be/9Be of 2.79 × 10–11.

3. Methods

3.1. Simple burial dating

Cosmogenic nuclide burial dating uses measurements of the concentration of ^{10}Be and ^{26}Al in samples that were exposed at surface prior to deposition and shielding from cosmic rays. Once buried the ^{26}Al and ^{10}Be content decrease due to radioactive decay, and the faster decay of ^{26}Al results in a decrease in the $^{26}Al/^{10}Be$. The $^{26}Al/^{10}Be$ ratio is used to derive a burial age assuming closed system behavior (Granger and Muzikar 2001; Granger, 2006, 2014).

The long-term concentration (Ni) of 26Al or 10Be in quartz that is exposed near the surface and then buried follows the relationship:

$$N_i = N_{i,inh} e^{(-t/\tau_i)} + N_{i,pb} \quad (1)$$

where subscript i represents either ^{26}Al or ^{10}Be, *inh* indicates inheritance prior to burial, t is burial age, τ is the radioactive mean life and *pb* indicates the total post-burial production. The radioactive mean life of ^{26}Al is 1.021 ± 0.024 Ma (Nishiizumi, 2004) and ^{10}Be is 2.005 ± 0.017 Ma (Chmeleff et al., 2010). In a landscape that is eroding steadily at a rate E, the inherited nuclide concentration is:

$$N_{i,inh} = P_n / (1/\tau_i + \rho E/\Lambda_n) + P_\mu / (1/\tau_i + \rho E/\Lambda_\mu) \quad (2)$$

where P_n, P_μ and Λ_n, Λ_μ are the production rates (atoms/g/yr) and penetration lengths (g/cm^2) due to neutrons and muons, respectively. Here, the muon production rate and penetration length including negative muon capture and fast muon reactions. The exponential penetration length for nucleon is 160 g/cm^2 (Masarik and Reedy, 1995), for negative muon and fast muon are 1510 g/cm^2 and 4320 g/cm^2 (Heisinger et al., 2002a, b). ρ indicates rock density (assumed 2.60 g/cm^3). Simple burial dating assumes that the sample was exposed at the surface with a high concentration of inherited nuclides and was then buried deeply enough (typically more than 10 m) so that post-burial production can safely be ignored. In this case, Eq. (1) simplifies to

$$N_{26}/N_{10} = (N_{26,inh}/N_{10,inh}) e^{-t(1/\tau_{26} - 1/\tau_{10})} \quad (3)$$

Eq. (2) and Eq. (3) can be solved iteratively for converging solution of burial age t and pre-burial erosion rate E. The current burial dating method limits range roughly between 0.1 and 5 Ma (Granger, 2014).

The basic premise of burial dating is that sediment is buried deep enough to avoid significant post-burial nuclide production and has a simple exposure history prior to burial. Thus, simple burial dating is ideal for dating cave sediments or thick fluvial deposits. However, complex exposure-burial histories prior to the final burial cannot be ruled out, making all burial ages maximum ages.

3.2. $^{26}Al/^{10}Be$ isochron-burial dating

Isochron burial dating is a variation of burial dating that eliminates signals from constant inheritance and post-burial concentrations. This method offers several advantages over the simple burial dating method; for instance, it allows sediments buried at depths as shallow as ~2 m to be dated (Schaller et al., 2016), and it allows the identification of samples that have a complex exposure-burial history prior to their final burial.

If all samples are from the same depth, the post-burial production of cosmogenic nuclide is common and can be taken as a constant. Then, Eq. (1) can be arranged into a single expression that relates N_{26} and N_{10}.

$$N_{26} = (N_{10} - N_{10,pb}) R_{inh} e^{-t(1/\tau_{26} - 1/\tau_{10})} + N_{26,pb} \quad (4)$$

where. $R_{inh} = N_{26,inh}/N_{10,inh} = (P_{26}/P_{10}) \cdot (1/\tau_{10} + E/\Lambda)/(1/\tau_{26} + E/\Lambda)$

Eq. (4) is the key to isochron burial dating and represents a straight line whose slope is determined only by the burial age t. It can be solved for a suite of samples, by modeling the inherited ratio R_{inh} and the relationship between $N_{26,pb}$ and $N_{10,pb}$. For inherited ratio, it is usually assumed that the production rate ratio is constant at a common value of 6.8, although it is possible that the ratio varies with latitude (Corbett et al., 2017), elevation (Argento et al., 2015) and depth (Heisinger et al., 2002a, b). Moreover, initial pre-burial $^{26}Al/^{10}Be$ ratio is also affected by altitude in the case of long pre-burial exposure ages (>100 ka) or low erosion rates (<1 m/Ma) (Blard et al., 2019). For shallow buried samples with significant post-burial nuclide production, generally two end-member scenarios can be considered (Zhao et al., 2016). The first is where samples have been buried beyond cosmic attenuation zone for the entire burial history and were recently exposed to cosmic rays. The second case is continuous buried at a constant depth. In this study, we considered the first scenario that post-burial cosmogenic nuclide production as recent exposure. In this case, the post-burial production can be described by:

$$N_{26,pb} = (P_{26,pb}/P_{10,pb}) N_{10,pb} \quad (5)$$

An isochron burial age requires simultaneously solving Eq. (4) and

Table 1
Sample locations and descriptions of the study cave morphology and sampling section.

Site	Sample	Elevation (m)	Location		Cave morphology					Sampling section and sample description
			Lat (°N)	Long (°E)	length (m)	width (m)	height (m)	description	type	
Libo	Dongge Cave (DGC)	650 ± 5	25°17.776″	108°02.397″	1100	3–55	2.5–30	A multi-level cave system contains three floors and the passage is near south to north.	watertable	Section is on the second floor and close to the No. 6 stalagmite. Fluvial sediments are covered by a 5 cm thick calcium layer. Diameters of gravels are 1–5 cm, cemented by the sand and clay.
	Yamen Cave (YMC)	587 ± 5	25°30′53.59″	107°55′37.65″	> 100	10–20	3–12	The secondary deposits are well developed in the cave, and the collapse is hardly observed.	watertable	The sampling site is on the left wall which ~1 m from the cave ground, with 80 cm thick that covered by a calcium layer. The gravels are tightly cemented, and diameter of less rounded sandstone pebble is 3–10 cm.
	Dongmen Cave (DMC)	575 ± 3	25°21′47.03″	108°03′23.00″	> 100	10–30	10–15	The cave is at the bottom of valley, cave passage is flat, there was a serious collapse phenomenon and the speleothem is less developed.	watertable	The section is located inside the cave about 60–70 m, ~3 m thick and pebbles are cemented tightly. The lithology of pebbles contains limestone, mudstone and sandstone. The diameter of rounded sandstone pebbles is 2–8 cm.
	Sancha River bank (SRB)	480 ± 5	25°18.307″	108°05.511″						The sampled sandstone pebbles are 5–10 cm in size.
Liuchong River	Dayan Cave sand (DYCs)	1345 ± 5	27°04′24.8″	105°11′04.5″	50	5	5	The passage is near east to west, and about 15° downward sloping. There developed a branch cave (20 m length, 1 m width and 1 m height) beside the north of main conduit, and parallel to the main conduit.	lateral erosion cave	The sampling section is at the bottom of the branch cave. The thickness of section is ~30 cm, and the breakdown is cover on the top of section. The lithology of pebble is primarily sandstone and cemented with sand.
	Shanshu Cave (SSC)	1281 ± 5	27°05′04.13″	105°09′47.08″	120	5	6	The cave is on the middle part of valley wall, and the passage is flat and near east to west.	watertable	The sampling site is located inside the cave about 50–60 m, with ~70 cm thick and pebbles are cemented tightly. The lithology of pebbles contains siltstone, mudstone and sandstone. The sampled well rounded sandstone pebbles is 3–5 cm in size.
	Terrace 1	1205 ± 6	27°02′38.2″	105°12′59.6″						The terrace surface is about 30–50 m wide and 200 m long. The section is about 2 m thick that overlying on the limestone bedrock. The lithology of pebbles is primarily limestone, mudstone, silicalite and a few of sandstone. The well rounded sandstone cobbles are collected at

(*continued on next page*)

Table 1 (*continued*)

Site	Sample	Elevation (m)	Location		Cave morphology					Sampling section and sample description
			Lat (°N)	Long (°E)	length (m)	width (m)	height (m)	description	type	
	Terrace 2	1215 ± 5	27°02′23.2″	105°12′53.0″						the horizon of ~150 cm under the surface. The section is about 6 m thick includes 2–3 m gravels overlying on the mudstone bedrock. The lithology of cobbles is primarily mudstone, limestone, sandstone and siltstone. The well rounded sandstone cobbles are collected at the bottom of gravels that close to bedrock.

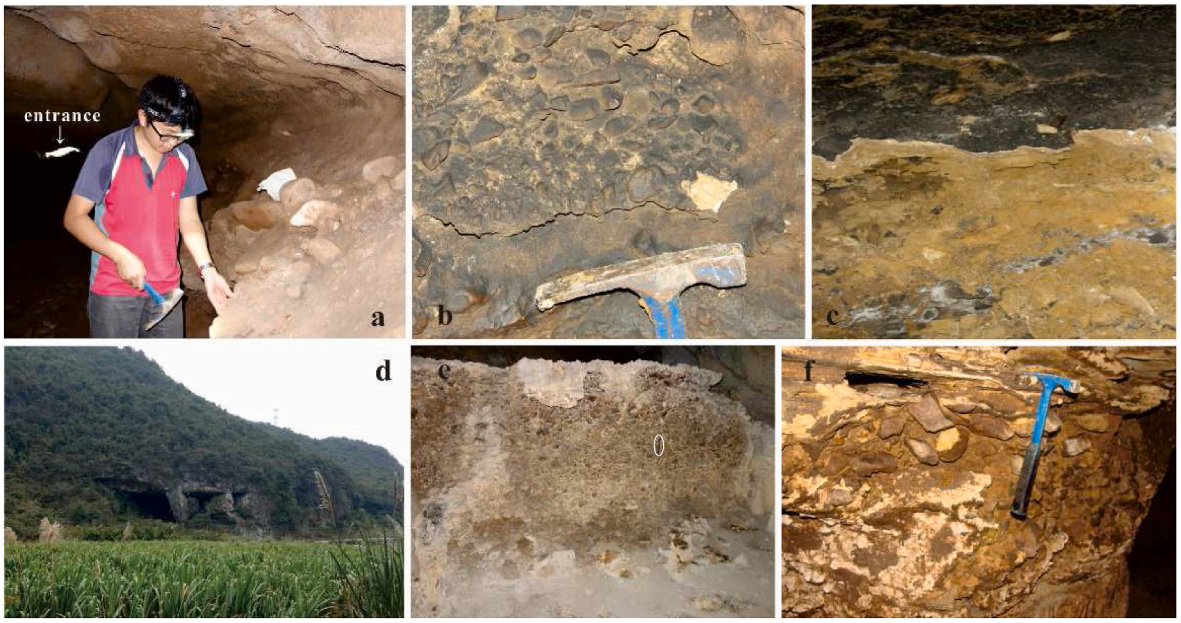

Fig. 3. Sediment sample locations in Guizhou caves. (a) A ~120 cm thick fluvial deposition along the passage of Shanshu Cave. A conglomerate sample was collected under the flowstone layer. (b) Gravels was capped by the calcite flowstone in the Dongge Cave. (c) A conglomerate sample was collected under the flowstone layer in the Dongge Cave. (d) Entrance of the Dongmen Cave at hillfoot in the Maolan River valley. (e) A thickness of 170 cm fluvial deposition section in the Dongmen Cave. Gravels are capped by a calcite flowstone. The white circle marks a pen with 15 cm. A conglomerate sample was collected under the flowstone layer in this section. (f) Gravel section in the Yamen Cave. A conglomerate sample was collected under the flowstone layer.

Eq. (5) by iteration (Balco and Rovey, 2008; Granger, 2014).

In this study, five clasts were collected from the same stratigraphical horizon. Based on the guidelines in Balco and Rovey (2008), Erlanger et al. (2012) and Zhao et al. (2016), Matlab code was used to calculate slopes and ages. Production rates of ^{10}Be and ^{26}Al were used with the scaling for altitude and latitude using Lal (1991) and Stone (2000). We assume $P_{26}/P_{10} = 6.80$ that is invariant with elevation. Sediment density was assumed as 2.60 g/cm^3. The regression is performed using the linear regression based on York et al. (2004).

4. Results

All results are shown in Table 2 and Fig. 5. The errors shown are 1σ calculated from AMS and ICP-OES uncertainties.

4.1. Burial age of cave sediments

The ^{26}Al/^{10}Be ratios of the cave samples range from 0.14 ± 0.03 to 5.62 ± 0.38 (Table 2). Apart from DGC all samples yielded burial ages ranging between 0.56 ± 0.16 Ma and 3.54 (+0.25/-0.22) Ma. The burial age of DYC sand is 2.44 (+0.23/-0.21) Ma, which is within 1σ of the age of pebble from the same cave (2.85 ± 0.21 Ma; Liu et al., 2013a). The modern bank sample of the Sancha River (SRB) has a finite burial age of 0.28 ± 0.13 Ma, indicating that the other samples from Libo may have experienced a short but complex burial history prior to their deposition in the caves. The DGC sample plots outside the burial zone in Fig. 5a. To constrain the burial age of DGC we measured the cosmogenic ^{21}Ne (Table 3 and Fig. 6). The non-atmospheric ^{21}Ne ((8.12 ± 2.93) × 10^6 atoms/g) in the sample includes an unresolved contribution from nucleogenic Ne. Thus, it represents an upper limit on the concentration of cosmogenic Ne in the sample and suggests that the burial age cannot exceed 1.23 ± 0.44 Ma. This ^{21}Ne-^{10}Be burial age is significantly different from the ^{26}Al–^{10}Be result. After re-calculation of ^{10}Be and ^{26}Al burial ages using ^{21}Ne concentration, we propose that the sample experienced a complex pre-burial history. Therefore, comparing with the unresolvable ^{26}Al–^{10}Be age, we suggest that ^{21}Ne-^{10}Be burial age of

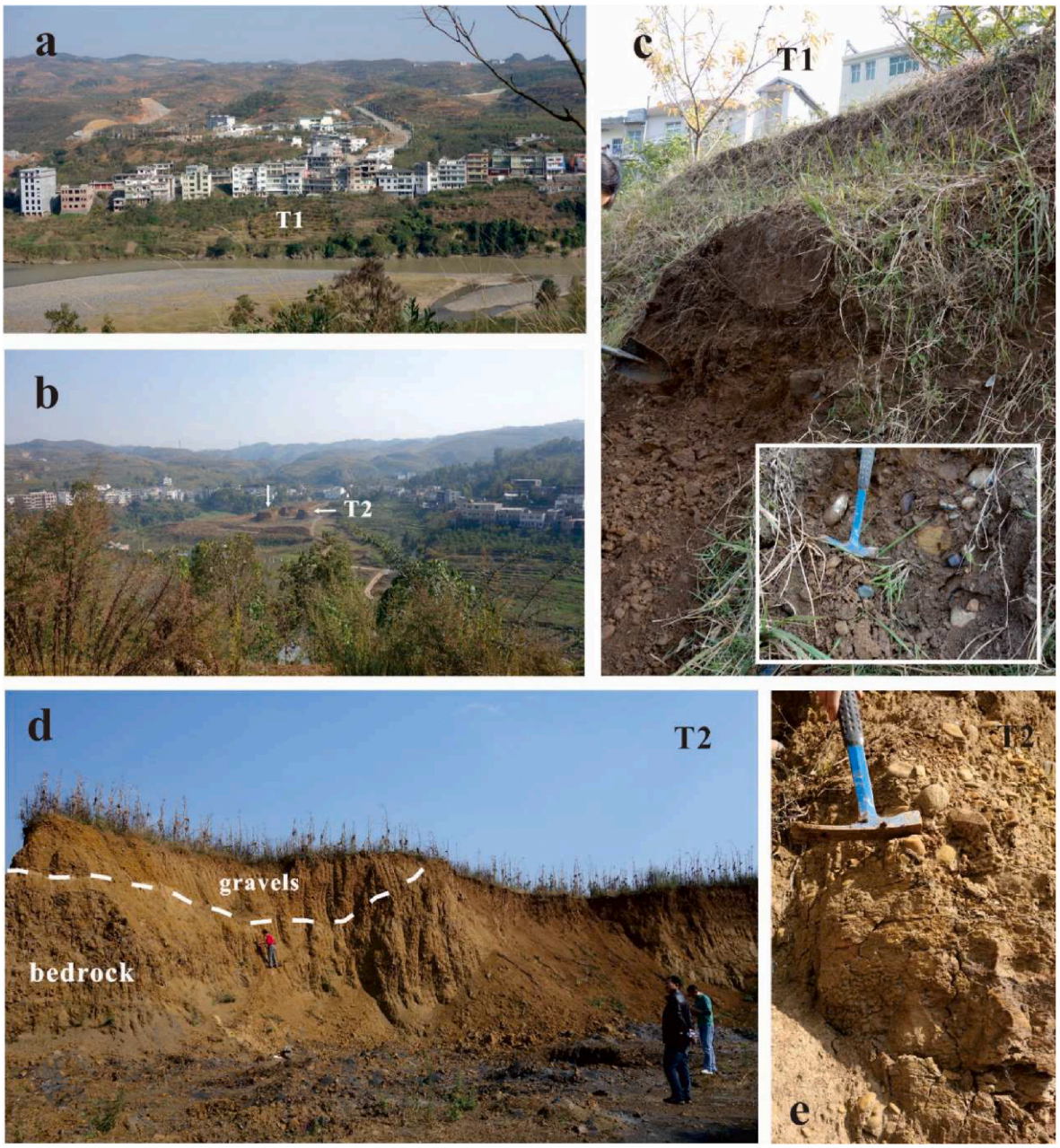

Fig. 4. Field pictures of the fluvial terraces in the Liuchong River. (a) Overview of T1 at Houchang village. (b) Overview of T2 at Pingzi village. (c) Sample location of T1: white box shows the excavated cobbles for isochron burial dating. (d) Recent exposed section of T2. (e) Boundary of gravels and mudstone bedrock of T2.

sample DGC is more reasonable and best represents its maximum burial age.

4.2. Isochron burial age of fluvial terraces

Fig. 5 shows the ^{10}Be and ^{26}Al data of the terraces from the Liuchong River. All data that plot below the initial line ($R_{init} = 6.8$) are compatible with simple exposure-burial histories. One sample from T1 (S1542) yielded $^{26}Al/^{10}Be = 7.22 \pm 0.70$. This may be explained by an initial $^{26}Al/^{10}Be$ that was dominated by muon production ($R_{init} > 7$). Excluding S1542, the slope of the line through the three T1 samples is 7.27 ± 0.56, which results in a negative age (Fig. 5b). Therefore, the isochron approach cannot be applied to T1. Five samples from T2, a higher and older terrace, show significant variation in radionuclide concentrations and define a well-constrained regression line with slope of 5.36 ± 0.30 and a deposition age of 0.41 ± 0.12 Ma (Fig. 5c). The MSWD (mean square of the weighted deviates) of 0.45 indicates good agreement of the apparent dispersion of five aliquots data with their individual measurement uncertainties.

5. Discussion

5.1. Fluvial incision history of the Liuchong River in NW Guizhou

Burial dating of sediments in the abandoned cave passages shows that the multi-level caves developed in step with the incision history of the Liuchong River throughout the Plio-Pleistocene. The burial ages increase with height above the modern river level as expected in the conceptual model of cave development (Table 4). SXC is the second highest cave level (level B) and yields a burial age of 1.46 Ma, albeit with large uncertainty (+1.32/-0.80) (Liu et al., 2013a). This may be best explained by a strong erosion events around deposition in the cave

Table 2
Cosmogenic nuclide ^{26}Al and ^{10}Be results of samples from study areas.

location	Sample ID	Quartz mass (g)	^{27}Al in quartz (ppm)	Carrier weight ^{9}Be (g)	^{26}Al/^{27}Al[a] (10^{-14})	^{10}Be/^{9}Be[a] (10^{-14})	Concentration (atoms/g)		^{26}Al/^{10}Be	Burial age* (Ma)	Erosion rate* (m/Ma)
							^{26}Al (10^{5})	^{10}Be (10^{4})			
Libo	DMC (S1519)	19.96	159 ± 5	0.1357	15.36 ± 0.64	15.23 ± 0.45	5.67 ± 0.41	10.85 ± 0.39	5.23 ± 0.42	0.56 ± 0.16	27 ± 3
	DGC (S1520)	20.18	350 ± 11	0.1364	1.64 ± 0.30	123.12 ± 1.58	1.22 ± 0.23	88.92 ± 1.96	0.14 ± 0.03	–	–
	YMC (S1521)	20.74	256 ± 8	0.1359	2.80 ± 0.28	20.87 ± 0.62	1.65 ± 0.19	14.42 ± 0.51	1.14 ± 0.14	3.54 (+0.25/-0.22)	4 ± 1
	SRB (S1522)	22.06	154 ± 5	0.1364	96.34 ± 2.53	91.04 ± 1.31	33.76 ± 2.17	60.08 ± 1.38	5.62 ± 0.38	0.28 ± 0.13	5 ± 1
Liuchong River	DYCs (S1517)	22.63	103 ± 4	0.1358	4.36 ± 0.37	8.06 ± 0.24	1.04 ± 0.11	4.97 ± 0.18	2.10 ± 0.23	2.44 (+0.23/-0.21)	47 ± 6
	SSC (S1518)	20.91	136 ± 5	0.1357	13.87 ± 0.69	16.41 ± 0.39	4.16 ± 0.32	11.17 ± 0.34	3.72 ± 0.31	1.25 (+0.17/-0.14)	38 ± 4
	Terrace T1										
	S1542	20.14	107 ± 4	0.2998	9.11 ± 0.44	4.49 ± 0.24	2.53 ± 0.19	3.50 ± 0.21	7.22 ± 0.70	–	–
	S1543	20.46	129 ± 4	0.3025	28.43 ± 0.83	17.66 ± 0.52	9.15 ± 0.60	14.53 ± 0.48	6.30 ± 0.46	0.17 ± 0.15	41 ± 4
	S1546	20.48	162 ± 5	0.2686	12.30 ± 0.46	11.30 ± 0.29	4.41 ± 0.27	8.13 ± 0.26	5.43 ± 0.38	0.49 ± 0.14	63 ± 5
	S1547	21.08	177 ± 6	0.2690	13.20 ± 0.49	13.31 ± 0.33	5.20 ± 0.33	9.36 ± 0.28	5.55 ± 0.39	0.44 ± 0.14	56 ± 5
	Terrace T2										
	S1544	21.39	140 ± 5	0.3033	85.04 ± 2.55	67.55 ± 1.05	30.17 ± 1.99	54.07 ± 1.15	5.58 ± 0.39	0.41 ± 0.12	
	S1548	21.79	187 ± 6	0.2600	24.70 ± 0.73	29.46 ± 0.72	10.30 ± 0.53	19.7 ± 0.57	5.23 ± 0.31		
	S1549	15.58	211 ± 7	0.2599	5.40 ± 0.28	5.25 ± 0.18	2.50 ± 0.20	4.59 ± 0.21	5.45 ± 0.50		
	S1550	15.67	219 ± 7	0.2602	8.54 ± 0.34	7.90 ± 0.22	4.14 ± 0.27	7.07 ± 0.25	5.85 ± 0.43		
	S1551	17.85	212 ± 7	0.2692	33.70 ± 0.98	35.41 ± 0.85	15.94 ± 0.83	30.0 ± 0.85	5.32 ± 0.32		

Note. *Local cosmogenic nuclide production rates in the Liuchong River were assumed constant for the basin and were calculated as $P_{n\&\mu,10} = 9.8$ atoms/(g·a) and $P_{n\&\mu,26} = 66.5$ atoms/(g·a) for a latitude of 30°N and an average upper drainage basin elevation of 1500 m. Local cosmogenic nuclide production rates in Libo were assumed constant for the basin and were calculated as $P_{n\&\mu,10} = 5.6$ atoms/(g·a) and $P_{n\&\mu,26} = 37.8$ atoms/(g·a) for a latitude of 25°N and an average drainage basin elevation of 750 m. All the calculations are based on the CRONUS Earth online calculator MATLAB code (Version 2.3).

[a] AMS blank ratios of Al (FISH) and Be (FVB) are zero and (2.21 ± 0.48) × 10^{-15}, respectively.

resulting from a significantly high pre-burial erosion rate of ~500 m/Ma (Liu et al., 2013a). The SXC age is not included in the following discussion because it may not necessarily reflect a meaningful age of passage formation. Sand sample of DYC from the third highest level (level C) yielded a burial age of 2.44 (+0.23/-0.21) Ma, which overlaps the pebble age (2.85 ± 0.21 Ma, Liu et al., 2013a). This confirms that the DYC passages were formed before 2.85 Ma and abandoned after 2.44 Ma. Consequently, the higher cave levels A and B, must have been formed before 2.85 Ma.

The river incision continued, and cave level D formed during the period of local base level stability. Sediments deposited in SSC at 80 m AML produced a burial age of 1.25 (+0.17/-0.14) Ma, suggesting that the cave passage was formed before this date. Thereafter level D was abandoned and the river began downcutting again. The level E cave passage at 50–60 m AML was formed before 0.75 ± 0.10 Ma on the Bizhi River and 0.49 ± 0.13 Ma on the Touwan River. Our data indicate that the passage development of level E is much older than the U-series age (0.16–0.18 Ma) from calcite flowstone (Yang, 1998). Speleothem can accumulate long after cave form and this age may significantly underestimate the cave age. Moreover, many Early Pleistocene mammalian fossil teeth have been found in Baeryan Cave located at an altitude approximately 1630 m, north of DSC (Zhao and Zhang, 2013). This cave is ~50 m above the local river and may correspond with level E. According to the mammalian fossil age, this cave is older than our age determination (0.75 Ma). However, there is possibility that the fossils have been transported into the young caves by river water and we consider that out burial age determination presents a more reliable age estimation of the time level E in this area.

The sixth and seventh levels of cave passages at 15–20 m AML and 5–10 m AML, respectively, are associated with discontinuous terraces of T2 and T1 along the Liuchong River. The burial age of T2 at Pingzi is well constrained by a clear trend line to 0.41 ± 0.12 Ma, suggesting that the corresponding cave passages of level F at 15 m AML were formed no later than 0.41 Ma. Then the Liuchong River incised again and formed level G, which is a hydrologically active cave at 5–10 m AML. The isochron approach cannot be applied to T1 pebbles. Individual cobble ages record burial ages from 0.17 ± 0.15 Ma to 0.49 ± 0.14 Ma (Table 2). This may reflect significant inherited ^{10}Be and ^{26}Al. Treating sample 1542 as a classic exposed sample, ^{10}Be and ^{26}Al exposure ages of 10.4 ± 1.1 ka and 12.2 ± 1.5 ka, respectively, are calculated from the CRONUS-Earth online calculators using version 2.3 (Balco et al., 2008). Time-independent production rates were scaled using factors from Lal (1991) and Stone (2000) and no shielding correction and erosion rate was considered. This age represents the minimum deposition age for T1 and is much younger than the U-series age of the speleothem from the nearby cave on the same level (48 ka; Yang, 1998). It appears that the Liuchong River abandoned level G after 10 ka and incised into the bedrock at the modern water table.

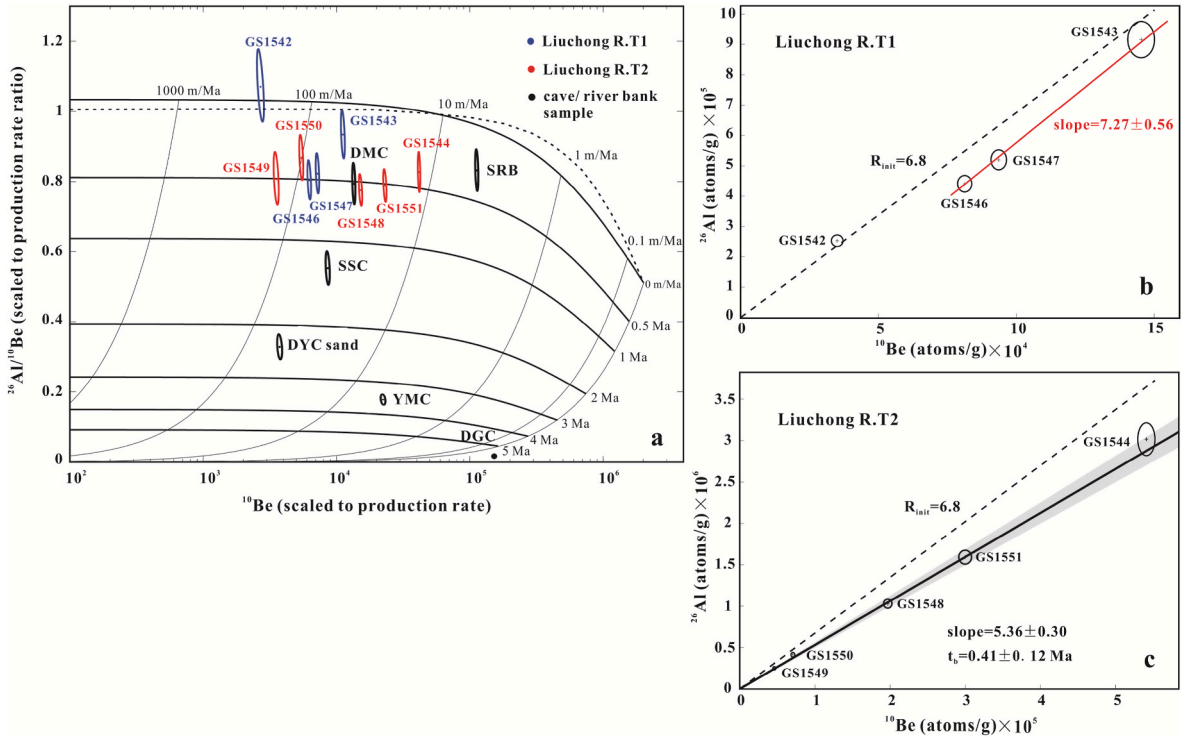

Fig. 5. Burial age data graphically displayed. (a) Cosmogenic nuclide data from cave sediments and fluvial terraces, shown on a logarithmic graph of ^{26}Al/^{10}Be versus ^{10}Be concentration. Labeling of sample acronyms as used in Table 1. (b) Isochron line for Terrace 1 of the Liuchong River. (c) Isochron line and age for Terrace 2 of the Liuchong River.

Table 3
Neon analysis results of quartz from the Dongge Cave in Libo.

Sample	^{20}Ne* (10^{10} atoms/g)	^{22}Ne/^{20}Ne*	^{21}Ne/^{20}Ne*	^{21}Ne* (10^6 atoms/g)	^{10}Be-^{21}Ne age[a] (Ma)
DGC	5.22 ± 0.01	0.1024 ± 0.0004	0.00311 ± 0.0006	8.12 ± 2.93	1.23 ± 0.44

Note. * Neon analysis was carried out at SUERC on 223.5 mg purified quartz. Sample was degassed at 1350 °C and analyzed using procedures of Codilean et al. (2008) using the CREU quartz (Vermeesch et al., 2015) as internal standard.

[a] Burial age was calculated following Ma et al. (2018), considering a bedrock density of 2.60 g/cm^3. Local cosmogenic^{21}Ne production rate was assumed constant for the basin and were calculated as P $_{n\&\mu,21}$ = 23.69 atoms/(g·a) for a latitude of 25°N and an average drainage basin elevation of 750 m.^{21}Ne/^{10}Be production rate ratio of 4.23 was assumed for spallation and muons (Kober et al., 2011). Radioactive decay constant of^{10}Be, which is the inverse of mean life ($\lambda = 1/\tau$), and we used value of (4.987 ± 0.043) × 10^{-7} per year (Chmeleff et al., 2010).

These burial ages suggest that samples from caves of level C–F in the Liuchong River experienced a simple exposure history before burial, and that recycling of late Quaternary sediments from the upstream catchments may have affected the sediments of Terrace 1 and the modern river. First, the burial ages obtained from pebbles and sands from DYC and DSC are in good agreement, suggesting that the sediments had a simple exposure history before burial. Second, the isochron line for Terrace 2 sediments implies no pre-burial history. However, the burial age of single cobble from Terrace 1 clearly shows that some recycled sediments were transported into the fluvial network. This continues to the present day as evident from the modern bank sediments of the Liuchong River and its tributary the Touwan River yielding burial ages of 0.26 ± 0.11 Ma and 0.35 ± 0.12 Ma, respectively (Liu et al., 2013a).

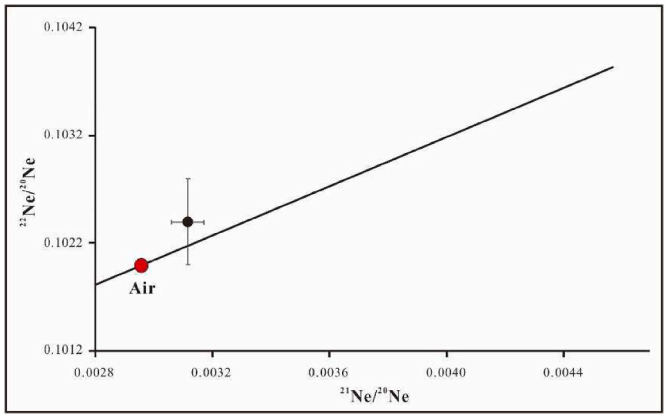

Fig. 6. Neon three isotope diagram for the Dongge Cave sample showing the Ne isotope ratios of the component.

5.2. Fluvial incision history of Libo in southern Guizhou

The abandonment of cave passages above the modern river allows the reconstruction of the fluvial incision history of the Libo karst landscape. The timing of cave formation in Libo obtained from this study is younger than proposed by Zhang et al. (2000), but much older than U–Th ages of speleothems (9.2–335 ka) in the Shenxian Cave in Dushan County, ~40 km northwest of Libo (Zhang and Zhao, 1985). The cave deposit burial ages extend back 3.54 Ma and, as expected, increase with elevation above the modern river (Table 4). Although no radiometric age could be determined to constrain the highest cave passages, levels A′ and B′ at 360–450 m AML, we infer that they must be older than 3.54 Ma from the age of a level C′ cave. YMC together with JDTC mark the third highest cave level (level C′, 150–160 m AML) in the area. The sediment burial age of YMC indicates that the river aggradation of level C′ is 3.54

Table 4
Fluvial chronology derived from the northeast and south Guizhou.

NW Guizhou Plateau (Liuchong River)					Southern Guizhou Plateau (Libo)			
Level	Height above local river (m)	Terrace	Cave	TCN age (Ma)	Level	Height above local river (m)	Cave	TCN age (Ma)
A	350		XC		A′	455	GYC	
B	220		SXC	1.46 (+1.32/-0.80)*	B′	360	BDC	
C	145		DYC	2.85 ± 0.21 (pebble)*	C′	162	YMC	3.54 (+0.25/-0.22)
				2.44 (+0.23/-0.21) (sand)		150	JDTC	
D	81		SSC	1.25 (+0.17/-0.14)	D′	85	DGC	1.23 ± 0.44
E	50		DSC	0.75 ± 0.10 (pebble)*	E′	43	BC	1.06 ± 0.23[a]
				0.69 ± 0.10 (sand) *				
	58		YTGC	0.49 ± 0.13*				
F	15	T2		0.41 ± 0.12	F′	10	DMC	0.56 ± 0.16
G	5	T1		0.01				

Note. * Data reported in Liu et al. (2013a).
[a] Cosmogenic nuclide burial age of Black Cave (BC) as assigned in Liu et al. (2013b).

(+0.25/-0.22) Ma and is the oldest cave deposit to date in our study. According to the morphology of these two caves, they require a longer period of passage development for the third level. A period of base-level stability followed the downcutting of the Maolan River, a fourth cave level passage formed at ~85 m AML in Libo (level D′). The resulting burial age of 1.23 ± 0.44 Ma determined by cosmogenic ^{10}Be and ^{21}Ne from DGC suggests that the passage formation for level D′ occurred before 1.23 Ma. This age also represents the aggradation age of sediments in the second floor passage of DGC. Therefore, the first floor passage formation of DGC at 115–125 m AML should have occurred between 1.23 and 3.54 Ma. A fourth incision episode cut the carbonate bedrock and abandoned level D′ after 1.23 Ma. The burial age of 1.06 ± 0.23 Ma for BC at 43 m AML, suggests that the river aggradation of lower level E' occurred at this time. The river subsequently abandoned the fifth level, and continued its incision and formed the sixth level before 0.56 ± 0.16 Ma (DMC). Finally, the Maolan River lowered again, reaching the current river level and ultimately forming an underground river at the end of the valley.

5.3. Comparison of the river aggradation and incision history in two study areas

Climate fluctuations and/or tectonic movements are important drivers of sediment aggradation and valley incision that have led to the development of river terraces and cave systems studied here. Unfortunately, the uncertainty associated with the burial ages are too large to allow robust correlation with established climate fluctuations (Fig. 7a). The burial ages of the cave sediments likely correspond to the terrace deposition ages of regionally important rivers, which are considered to trace regional tectonic uplift. For example, ~1.2 Ma, ~0.8 Ma and ~0.5 Ma terraces are widely recorded along the Yellow River and the Yangtze River and their tributaries (e.g. Li et al., 2001; Hu et al., 2011; He et al., 2015).

Good agreement exists between the cave levels in southern Guizhou, and the caves and terraces within the NW Guizhou Plateau (Table 4 and Fig. 7b). The burial ages for the D/D′, E/E′ and F/F' levels in both regions correspond well indicating that the two margins have a similar river aggradation and incision history over the last 1.25 Ma, and have experienced four episodic uplifts since 3.5 Ma.

Plotting the burial age data against the elevation above the current river provides an insight into the regional landscape evolution (Fig. 7b).

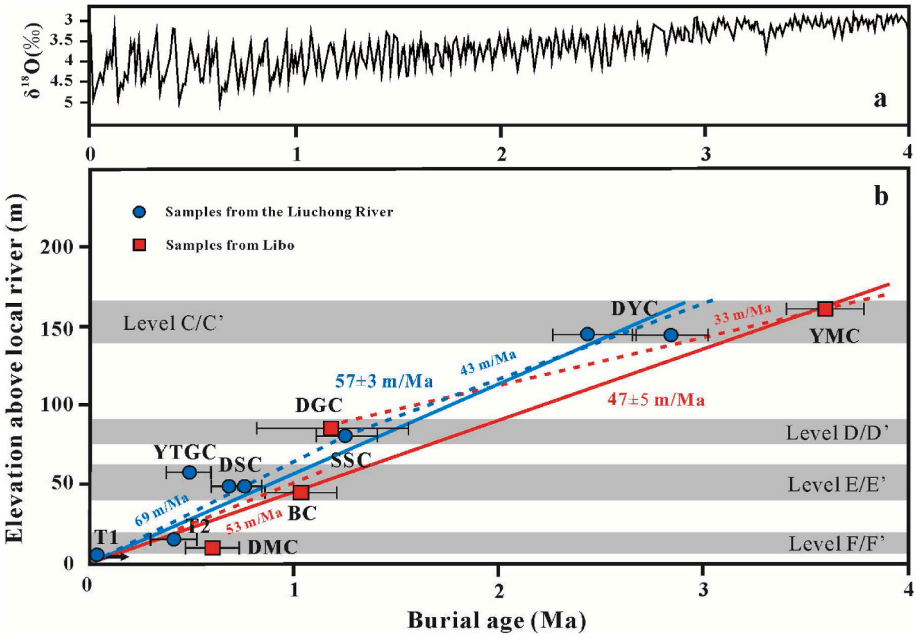

Fig. 7. (a) Benthic δ18O record track warm and cold stages (Lisiecki and Raymo, 2005); (b) Burial ages and river incision history from caves in both study areas. The blue and red lines represent river incision rates in the Liuchong River and Libo, respectively. Solid line denotes the average incision rate from the two regions and the dashed line denotes the incision rate at different time periods.

The long-term incision rate of the Liuchong River is 57 ± 3 m/Ma, calculated from the six caves and two terraces dated in this study. This is significantly lower than the previous estimate of 480 m/Ma (Liu et al., 2013a). Using the altitude of the modern Liuchong River as the local base level for all the samples in the previous study means that height above local river is overestimated, especially the high elevation caves on the tributaries. Consequently, the river incision rates are over-estimated. Here we use the elevation of each cave relative to the local river, to calculate the river incision rate.

The long-term late Cenozoic incision rate determined from dated caves in Libo of 47 ± 5 m/Ma is lower than the 57 ± 3 m/Ma determined for the Liuchong River (Fig. 7b). These uplift rates are significantly different to those determined for the inner and outer margins of the Tibetan Plateau. The linear distance between the two study areas in Guizhou is approximately 300 km, while the uplift rate difference is about 10 m/Ma. In the inner part of the SE Tibetan margin, the uplift rates and rate differences are much larger. For example, in the Lancang Jiang (Mekong), the Tu'e reaches experienced uplift of 940 m/Ma while the uplift of the Changdu reaches 600 km to the south experienced 350 m/Ma (Fig. 8). This is because that the Guizhou region is farther southeast along the Tibetan Plateau margin from Tibet than those areas, and thus experienced less and more uniform surface uplift.

Sediment burial ages in the Liuchong River reveal a relatively slow incision rate of 43 m/Ma from 2.85 to 1.25 Ma, followed by a faster incision rate of 69 m/Ma from 1.25 Ma to the present. A similar pattern is recorded in the Libo area, where incision rates of 33 m/Ma from 3.54 to 1.23 Ma, increased to 53 m/Ma after this time. The incision rate increase is probably resulted from an accelerated tectonic uplift of the Tibetan Plateau that is widely observed in the north and south China (e.g. Jiang and Wu, 1998; Li et al., 2014).

The longitudinal river profiles reflect the interaction between surface uplift and the dynamics of river incision, and hence should record the local and regional tectonic history (Royden and Perron, 2013). Fig. 8 shows the longitudinal profiles of the bedrock rivers in this study. All the river profiles have a concave-up shape. Knickpoints are present in all rivers, for example the Sancha River in Libo area (Fig. 8c). They are mainly vertical-step knickpoints which are caused by lithology contrasts or faults. This character suggests that the rivers are in a transient condition. This would not affect the incision rate calculation derived from the burial age and height above river.

5.4. Regional comparison

The multi-level caves and alluvial terraces are the result of tectonic uplift and base level lowering. When the river incision is equal to the rock uplift, the incision rate calculated from terraces or caves sediment burial ages represents the rock uplift rate. Thus, fluvial incision and terraces may be the result of tectonic uplift, and the uplift rate calculated from elevated terraces or caves merely yields the maximum uplift value (Kiden and Tornqvist, 1998). The maximum rock uplift rates for northwestern and southern Guizhou derived from cave and terrace sediments in this study (57 m/Ma and 47 m/Ma) are considerably slower than Plio-Pleistocene exhumation rate derived from low temperature thermochronology (Luo et al., 2009), indicating the highland landscape of the Guizhou Plateau had already developed before the Quaternary. Moreover, our data show that the Liuchong River has down cut only 145 m (or rock uplift, not considering isostatic uplift) in the past 2.85 Ma, firmly refuting the hypotheses of 1–2 km of Quaternary surface uplift (Lin, 1993). Recent paleo-elevation reconstruction in Yunnan Plateau suggest that NW Yunnan topography was established before ~40 Ma, and ~13 Ma in SE Yunnan (Hoke et al., 2014; Li et al., 2015; Wu et al., 2018). Paleo-elevation estimates in Guizhou region are hampered by the lack of suitable material, but we infer that prototype of the Yungui Plateau may had occurred at least before the Late Pliocene.

Although river incision is only one of the processes that compensates for tectonic uplift, the river incision rate decreases from the inner Tibetan Plateau to the Guangxi Basin and shows an uplift variation from the plateau interior to the geomorphic margin and plain (Fig. 9). These studies show that river incision or related uplift is has been around ~80 m/Ma since ~1.8 Ma (Zhu, 2012) in the inner Tibetan Plateau, and is abruptly increased 2–5 times to 150–400 m/Ma in the last ~1 Ma (Zhao et al., 2013; He et al., 2015; Wei, 2016; Liu, 2018; Su et al., 2019). At the adjacent plateau margins uplift reached 1100–1800 m/Ma since late Quaternary in the active neotectonics zone, for example the Longmen Shan (Li et al., 2005). The average river incision rate rapidly decreases to 50–60 m/Ma (this study) in the outer margin and finally to ~20 m/Ma in the plain further east (Williams, 1987). This trend is conflicts with the annual temperature and precipitation variation tendency, suggesting that the tectonics is the main trigger activating the late Cenozoic river incision in the SW China although possible role of enhanced erosional efficiency by the climate (Asian monsoon) change.

It is important to note that the river incision rates listed above were estimated over different timescales. Some uplift rates cover millions of years timescale, including the Yarlung Zangbo Jiang, the Yalong Jiang, the Dadu River, and the Jinsha Jiang, but the incision rates from other studies cover shorter timescale (for example, data of the Lancang Jiang are in the recent ~0.6 Ma). This difference can lead to a phenomenon referred to as the "Sadler effect" that induces an apparent decrease in the fluvial incision rate over longer timescales (Sadler, 1981; Nativ and Turowski, 2020). Using Equation 11 in Nativ and Turowski (2020) to

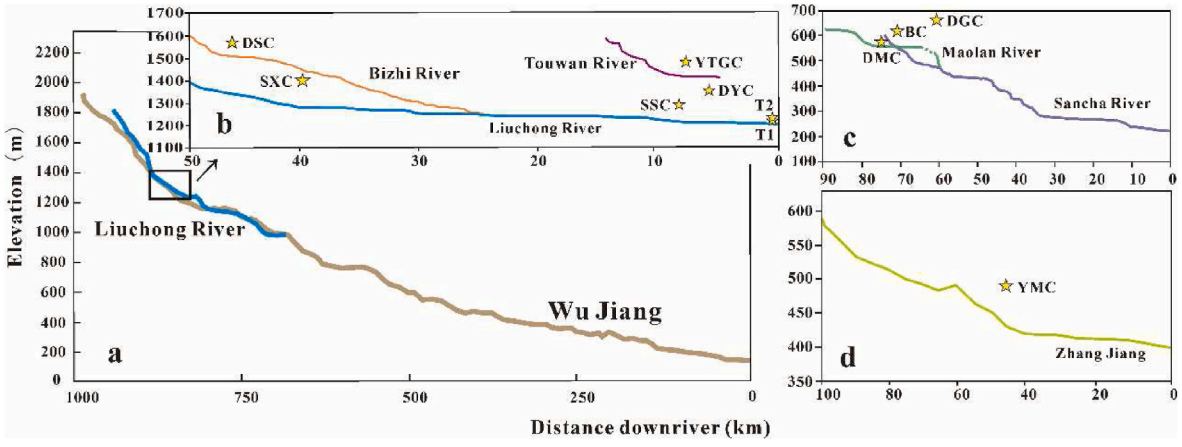

Fig. 8. The longitudinal profile of the studied rivers in the Guizhou Plateau. All the parameters were extracted from 90 m resolution DEM SRTM. Dated cave or fluvial terrace was marked with star. (a) The Wu Jiang and the Liuchong River; (b)studied section of the Liuchong River and its two tributaries the Bizhi River and the Touwan River; (c) The Sancha River and its tributary the Maolan River in Libo area; (d) The Zhang Jiang in Libo area.

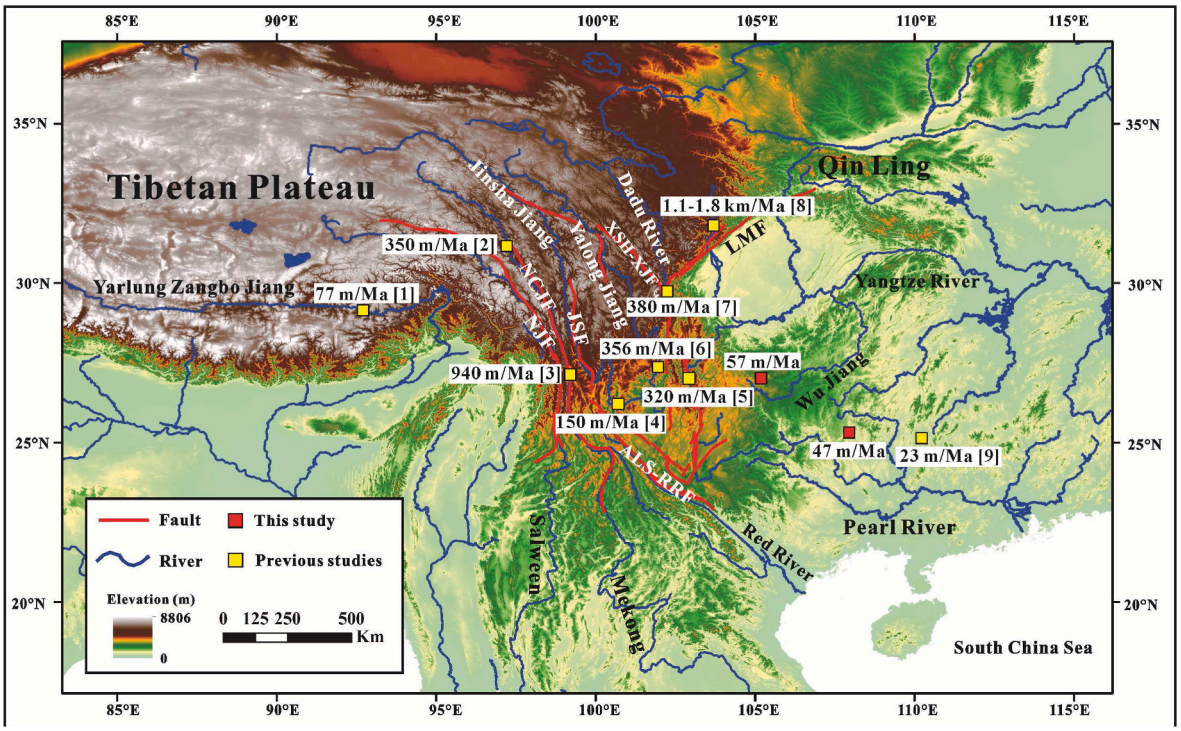

Fig. 9. Simplified tectonic and regional topography of the eastern and southeastern Tibetan Plateau showing the river incision change around the plateau and margin areas. Abbreviations: ALS-RRF = Ailaoshan-Red River Fault, LMF = Longmenshan Fault, NCJF=Nancangjiang Fault, NJF=Nujiang Fault, XSH-XJF = Xianshuihe-Xiaojiang Fault. Reference codes are [1] = Zhu (2012), [2] = Wei , 2016, [3] = Wang et al. (1999), [4] = Su et al. (2019), [5] = Liu (2018), [6] = He et al. (2015), [7] = Zhao et al. (2013), [8] = Li et al. (2005), [9] = Williams (1987).

evaluate the bias due to the "Sadler effect" by using the 99th percentile, a comparison between terrace/cave-derived incision rates that integrate contrasting ages of 1 Ma and 3 Ma, 600 ka and 3 Ma, would yield a bias of a factor of 2 and 3 solely due to a timescale dependence. This result suggests that our incision rates measured over a 3 Ma timescale may be underestimated by two or three times, compared to those from, such as the Yalong Jiang which apply to the last ~1 million years, and the Lancang Jiang estimated over ~0.6 Ma timescale. However, even considering the "Sadler effect", the incision rates from the Guizhou Plateau are still significantly lower than inner parts of the southeastern margin of the Tibetan Plateau.

6. Conclusions

The landscape evolution of Guizhou is poorly constrained in the past that could only suggest the relative ages of landscape features such as cave levels. Using new sediment burial ages, we determine the incision rate of the two main rivers draining north and south, as well as documenting multiphase plateau incision history. The cosmogenic ^{10}Be–^{26}Al burial ages determined from flights of caves and terraces in the Liuchong River in NW Guizhou and Libo in southern Guizhou range between 0.41 ± 0.12 Ma and 3.54 + 0.25/-0.22 Ma. Although the rock uplift rate derived from the river incision rate of NW Guizhou (57 m/Ma) has been faster than that of the southern margin (47 m/Ma), but the small difference of uplift rate suggests that the Guizhou Plateau has experienced a relative uniform surface uplift during the Late Cenozoic, and the highland geography of the Guizhou Plateau has already occurred before the Quaternary.

Declaration of competing interest

The authors declared that they have NO conflicts of interest to this work. We declare that we do not have any commercial or associative interest that represents a conflict of interest in connection with the work submitted.

Acknowledgments

We are grateful to Yan Ma at Institute of Geology, China Earthquake Administration for the neon isotope measurement. We also appreciate the help of María Miguens-Rodríguez at SUERC in sample preparation in the laboratory. This work was supported by the Strategic Priority Research Program of the Chinese Academy of Sciences (XDB40020300) and National Natural Science Foundation of China (41473055, 41401009).

References

An, Z.S., Clemens, S.C., Shen, J., Qiang, X.K., Jin, Z.D., Sun, Y.B., et al., 2011. Glacial-interglacial Indian summer monsoon dynamics. Science 333, 719–723.
Argento, D.C., Stone, J.O., Reedy, R.C., O'Brien, K., 2015. Physics-based modeling of cosmogenic nuclides part I-Radiation transport methods and new insights. Quat. Geochronol. 26, 29–43.
Balco, G., Rovey, C.W., 2008. An isochron method for cosmogenic-nuclide dating of buried soils and sediments. Am. J. Sci. 308, 1083–1114.
Balco, G., Stone, J.O., Lifton, N.A., Dunai, T.J., 2008. A complete and easily accessible means of calculating surface exposure ages or erosion rates from Be-10 and Al-26 measurements. Quat. Geochronol. 3, 174–195.
Blard, P.H., Lupker, M., Rousseau, M., 2019. Paired-cosmogenic nuclide paleoaltimetry. Earth Planet Sci. Lett. 515, 271–282.
Cao, K., Wang, G., Leloup, P.H., Mahéo, G., Xu, Y., van der Beek, P.A., et al., 2019. Oligocene-Early Miocene topographic relief generation of southeastern Tibet triggered by thrusting. Tectonics 38, 374–391.
Chmeleff, J., Blanckenburg, F., Kossert, K., Jakob, D., 2010. Determination of the 10Be half-life by multicollector ICP-MS and liquid scintillation counting. Nucl. Instrum. Methods Phys. Res., Sect. B 268, 192–199.
Clark, M.K., Royden, L.H., 2000. Topographic ooze: building the eastern margin of Tibet by lower crustal flow. Geology 28, 703–706.
Clark, M.K., Schoenbohm, L.M., Royden, L.H., Whipple, K.X., Burchfiel, B.C., Zhang, X., Tang, W., Wang, E., Chen, L., 2004. Surface uplift, tectonics, and erosion of eastern Tibet from large-scale drainage patterns. Tectonics 23, 1–20.
Clark, M.K., House, M.A., Royden, L.H., Whipple, K.X., Burchfiel, B.C., Zhang, X., Tang, W., 2005. Late cenozoic uplift of southeastern Tibet. Geology 33, 525–528.

Clift, P.D., Sun, Z., 2006. The Sedimentary and Tectonic Evolution of the Yinggehai-Song Hong basin and the southern Hainan margin, South China Sea: implications for Tibetan uplift and monsoon intensification. J. Geophys. Res. 111, B06405.
Codilean, A.T., Bishop, P., Stuart, F.M., Hoey, T.B., Fabel, D., Freeman, S.P.H.T., 2008. Single-grain cosmogenic 21Ne concentrations in fluvial sediments reveal spatially variable erosion rates. Geology 36, 159–162.
Corbett, L.B., Bierman, P.R., Rood, D.H., Caffee, M.W., Lifton, N.A., Woodruff, T.E., 2017. Cosmogenic 26Al/10Be surface production ratio in Greenland. Geophys. Res. Lett. 44, 1350–1359.
Erlanger, E.D., Granger, D.E., Gibbon, R.J., 2012. Rock uplift rates in South Africa from isochron burial dating of fluvial and marine terraces. Geology 40, 1019–1022.
GBGMR (Guizhou Bureau of Geology and Mineral Resource), 1987. Regional Geology of Guizhou Province. Geology Press, Beijing, pp. 599–631.
Granger, D.E., 2006. A review of burial dating methods using 26Al and 10Be. GSA (Geol. Soc. Am.) Spec. Pap. (Reg. Stud.) 415, 1–16.
Granger, D.E., 2014. Cosmogenic nuclide burial dating in archaeology and paleoanthropology. In: Turekian, K., Holland, H. (Eds.), Treatise on Geochemistry, second ed., vol. 14. Elsevier Publishing, pp. 81–97.
Granger, D.E., Muzikar, P.F., 2001. Dating sediment burial with in situ-produced cosmogenic muclides: theory, techniques, and limitations. Earth Planet Sci. Lett. 188, 269–281.
He, Z.X., Zhang, X.J., Bao, S.Y., Qiao, Y.S., Sheng, Y.Y., Liu, X.T., et al., 2015. Multiple climate cycles imprinted on regional uplift-controlled fluvial terraces in the lower Yalong River and Anning River, SE Tibetan Plateau. Geomorphology 250, 95–112.
Heisinger, B., Lal, D., Jull, A., Kubik, P., Ivy-Ochs, S., Neumaier, S., et al., 2002a. Production of selected cosmogenic radionuclides by muons: 1. Fast muons. Earth Planet Sci. Lett. 200, 345–355.
Heisinger, B., Lal, D., Jull, A., Kubik, P., Ivy-Ochs, S., Knie, K., Nolte, E., 2002b. Production of selected cosmogenic radionuclides by muons: 2. Capture of negative muons. Earth Planet Sci. Lett. 200, 357–369.
Henck, A.C., Huntington, K.W., Stone, J.O., Montgomery, D.R., Hallet, B., 2011. Spatial controls on erosion in the three rivers region, southeastern Tibet and southwestern China. Earth Planet Sci. Lett. 303, 71–83.
Hetzel, R., Niedermann, S., Tao, M.X., Kubik, P.W., Strecker, M.R., 2006. Climate versus tectonic control on river incision at the margin of NE Tibet: 10Be exposure dating of river terraces at the mountain front of the Qilian Shan. J. Geophys. Res. 111, F03012.
Hoke, G.D., Liu-Zeng, J., Hren, M.T., Wissink, G.K., Garzione, C.N., 2014. Stable isotopes reveal high southeast Tibetan Plateau margin since the Paleogene. Earth Planet Sci. Lett. 394, 270–278.
Hu, X.F., Kirby, E., Pan, B.T., Granger, D.E., Su, H., 2011. Cosmogenic burial ages reveal sediment reservoir dynamics along the Yellow River, China. Geology 39, 839–842.
Hubbard, Judith, Shaw H., John, 2009. Uplift of the Longmen Shan and Tibetan plateau, and the 2008 Wenchuan (M=7.9) earthquake. Nature 458, 194–197. https://doi.org/10.1038/nature07837.
Jiang, F.C., Wu, X.H., 1998. Late Cenozoic tectonic movement in geomorphologic boundary belt of southeastern Qinghai-Xizang Plateau. J. Chengdu Univ. Technol. (Sci. Technol. Ed.) 25, 162–168.
Kiden, P., Tornqvist, T.E., 1998. Can river terrace flights be used to quantify Quaternary tectonic uplift rates? J. Quat. Sci. 13, 573–575.
Kober, F., Alfimov, V., Ivy-Ochs, S., Kubik, P.W., Wieler, R., 2011. The cosmogenic 21Ne production rate in quartz evaluated on a large set of existing 21Ne–^{10}Be data. Earth Planet Sci. Lett. 302, 163–171.
Kohl, C.P., Nishiizumi, K., 1992. Chemical isolation of quartz for measurement of in-situ-produced cosmogenic nuclides. Geochem. Cosmochim. Acta 56, 3583–3587.
Kong, F.C., Yang, R.D., Han, X.T., 2010. Analysis on the river terrace sediment in Quaternary period of Guizhou Province. Guizhou Geol. 27, 91–94.
Lal, D., 1991. Cosmic ray labeling of erosion surfaces: in situ nuclide production rates and erosion models. Earth Planet Sci. Lett. 104, 424–439.
Lei, Y.L., Zhong, D.L., Jia, C.Z., Ji, J.Q., Zhang, J., 2008. Late Cenozoic differential uplift-exhumation of batholiths and propagation of uplift recorded by fission track thermochronology in Chayu area, the southeast margin of the Tibetan Plateau. Acta Petrol. Sin. 24, 384–394.
Li, J.J., Xie, S.Y., Kuang, M.S., 2001. Geomorphic evolution of the Yangtze Gorges and the time of their formation. Geomorphology 41, 125–135.
Li, Y., Cao, S.Y., Zhou, R.J., 2005. Late Cenozoic Minjiang incision rate and its constraint on the uplift of the eastern margin of the Tibetan Plateau. Acta Geol. Sin. 79, 28–37.
Li, J.J., Fang, X.M., song, C.H., Pan, B.T., Ma, Y.Z., Yan, M.D., 2014. Late Miocene–Quaternary rapid stepwise uplift of the NE Tibetan Plateau and its effects on climatic and environmental changes. Quat. Res. 81, 400–423.
Li, S.Y., Currie, B.S., Rowley, D.B., Ingalls, M., 2015. Cenozoic paleoaltimetry of the SE margin of the Tibetan Plateau: constraints on the tectonic evolution of the region. Earth Planet Sci. Lett. 432, 415–424.
Lin, S.J., 1993. The main features of tectonic movement of late Cenozoic Era in Guizhou. Geol. Guizhou 10, 10–17.
Lin, S.J., Zhou, Q.Y., Chen, P.Y., 1994. The Upper Cenozoic of Guizhou. Guizhou Science and Technology Press, Guiyang, pp. 66–126.
Lisiecki, L.E., Raymo, M.E., 2005. A Pliocene-Pleistocene stack of 57 globally distributed benthic d^{18}O records. Paleoceanography 20, PA1003.
Liu, F.L., 2018. Geomorphological Evolution and Valley Development of the Lower Jinsha River during Late Cenozoic. Doctoral dissertation. Lanzhou University, Lanzhou.
Liu, Y., Wang, S.J., Xu, S., Fabel, D., Liu, X.M., Zhang, X.B., et al., 2013a. New evidence for the incision history of the Liuchong River, Southwest China, from cosmogenic 26Al/10Be burial ages in cave sediments. J. Asian Earth Sci. 73, 274–283.
Liu, Y., Wang, S.J., Liu, X.M., Xu, S., Fabel, D., Luo, W.J., 2013b. Cosmogenic nuclides 26Al and 10Be burial age of black cave sediments, Libo of Guizhou, China. Quat. Sci. 33, 1–8.
Luo, K.P., Liu, G.X., Wang, J.Y., 2009. Fission track analysis of meso-cenozoic uplift and denudation in Jinsha area, the qianzhong uplift. Marine Origin Petrol. Geol. 14, 61–64.
Ma, Y., Wang, W.T., Zheng, D.W., Zhang, H.P., Pang, J.Z., Wu, Y., et al., 2018. Mid-Miocene cosmogenic upper limit for 10Be/21Ne burial age. Quat. Geochronol. 48, 72–79.
Masarik, J., Reedy, R.C., 1995. Terrestrial cosmogenic nuclide production systematic calculated from numerical simulations. Earth Planet Sci. Lett. 136, 381–395.
Molnar, P., Tapponnier, P., 1975. Cenozoic tectonics of Asia: effects of continental collision. Science 189, 419–426.
Molnar, P., England, P., Martinod, J., 1993. Mantle dynamics, the uplift of the Tibetan Plateau and the Indian monsoon. Rev. Geophys. 31, 357–396.
Nativ, R., Turowski, M., 2020. Site dependence of fluvial incision rate scaling with timescale. J. Geophys. Res.: Earth Surf. 125, e2020JF005808 https://doi.org/10.1029/2020JF005808.
Nishiizumi, K., 2004. Preparation of 26Al AMS standards. Nucl. Instrum. Methods Phys. Res., Sect. B 223, 388–392.
Partriage, T.C., Granger, D.E., Caffee, M.W., Clarke, R.J., 2003. Lower Pliocene hominid remains from sterkfontein. Science 300, 607–612.
Royden, L., Perron, J.T., 2013. Solutions of the stream power equation and application to the elevation of river longitudinal profiles. J. Geophys. Res.: Earth Surf. 118, 497–518.
Sadler, P.M., 1981. Sediment accumulation rates and the completeness of stratigraphic sections. J. Geol. 89, 569–584. https://doi.org/10.1086/628623.
Schaller, M., Ehlers, T.A., Stor, T., Torrent, J., Lobato, L., Christl, M., Vockenhuber, C., 2016. Timing of European fluvial terrace formation and incision rates constrained by cosmogenic nuclide dating. Earth Planet Sci. Lett. 451, 221–231.
Schoenbohm, L.M., Burchfiel, B.C., Chen, L.Z., 2006. Propagation of surface uplift, lower crustal flow, and Cenozoic tectonics of the southeast margin of the Tibetan Plateau. Geology 34, 813–816.
Sol, S., Meltzer, A., Bürgmann, R., van der Hilst, R.D., King, R., Chen, Z., Koons, P.O., Lev, E., Liu, Y.P., Zeitler, P.K., Zhang, X., Zhang, J., Zurek, B., 2007. Geodynamics of the southeastern Tibetan Plateau from seismic anisotropy and geodesy. Geology 35, 563–566.
Stock, G.M., Granger, D.E., Sasowsky, I.D., Anderson, R.S., Finkel, R.C., 2005. Comparison of U-Th, paleomagnetism, and cosmogenic burial methods for dating caves: implications for landscape evolution studies. Earth Planet Sci. Lett. 236, 388–403.
Stone, J., 2000. Air pressure and cosmogenic isotope production. J. Geophys. Res. 105, 23753–23759.
Su, H., Dong, M., Hu, Z.B., 2019. Late Miocene birth of the Middle Jinsha River revealed by the fluvial incision rate. Global Planet. Change 183, 103002.
Vermeesch, P., Balco, G., Blard, P.H., Dunai, T., Kober, F., Niedermann, S., et al., 2015. Interlaboratory comparison of cosmogenic 21Ne in quartz. Quat. Geochronol. 26, 20–28.
Wang, E., Kirby, E., Furlong P., K., van Soest, M., Xu, G., Shi, X., Kamp J.J., P., Hodges V., K., 2012. Two-phase growth of high topography in eastern Tibet during the Cenozoic. Nature geoscience 5, 640–645. https://doi.org/10.1038/NGEO1538.
Wang, G.Z., Wang, C.S., Liu, D.Z., Liu, S.G., 1999. Uplift and denudation of the western Yunnan Plateau in quaternary. Mar. Geol. Quat. Geol. 19, 67–74.
Wang, G.Z., Wang, C.S., Zeng, Y.F., Zhao, X.K., 2000. The uplift of the western Yunnan Plateau and sedimentary response of the yinggehai basin. Acta Sedimentol. Sin. 18, 234–240.
Wang, C.Y., Chan, W.W., Mooney, W.D., 2003. Three-dimensional velocity structure of crust and upper mantle in southwestern China and its tectonic implications. J. Geophys. Res. 108, 2442.
Wang, C.S., Zhao, X.X., Liu, Z.F., Lippert, P.C., Graham, S.A., Coe, R.S., et al., 2008. Constraints on the early uplift history of the Tibetan Plateau. Proc. Natl. Acad. Sci. Unit. States Am. 105, 4987–4992.
Wei, Y.G., 2016. River Terrace Sequences in Upstream of Lancang River and its Relevance with Structural Uplifting, (Master's Thesis). Liaoning Normal University, Shenyang.
Williams, P.W., 1987. Geomorphic inheritance and the development of tower karst. Earth Surf. Process. Landforms 12, 453–465.
Wu, J., Zhang, K.X., Xu, Y.D., Wang, G.C., Garzione, C.N., Eiler, J., Leloup, P.H., Sorrel, P., Maheo, G., 2018. Paleoelevations in the Jianchuan Basin of the southeastern Tibetan Plateau based on stable isotope and pollen grain analyses. Palaeogeogr. Palaeoclimatol. Palaeoecol. 510, 93–108.
Xu, S., Freeman, S., Rood, D.H., Shanks, R.P., 2015. Decadal 10Be, 26Al and 36Cl QA measurements on the SUERC 5MV accelerator mass spectrometer. Nucl. Instrum. Methods Phys. Res. B 361, 39–42.
Yang, H.R., 1944. Landform development of middle part of Guizhou. Acta Geograph. Sin. 11.
Yang, M.D., 1998. Characteristics and hydrodynamic conditions of cave development in karst gorge districts. Carsol. Sin./Zhong Guo Yan Rong 17, 187–195.
Yao, H.J., Beghein, C., Van der Hilst, R.D., 2008. Surface wave array tomography in SE Tibet from ambient seismic noise and two-station analysis-II. Crustal and upper-mantle structure. Geophys. J. Int. 173, 205–219.
York, D., Evensen, N.M., Martinez, M.L., Delgado, J.D.B., 2004. Unified equations for the slope, intercept, and standard errors of the best straight line. Am. J. Phys. 72, 367–375.

Yuan, D.X., Cheng, H., Edwards, R.L., Dykoski, C.A., Kelly, M.J., Zhang, M.L., et al., 2004. Timing, duration, and transitions of the last interglacial Asian monsoon. Science 304, 575–578.
Zhang, S.Y., Zhao, S.S., 1985. Radioactive Dating of Shenxian Cave Sediments from Dushan, Guizhou. Karst Landform and Cave. Science Press, Beijing, pp. 113–116.
Zhang, M.L., Lin, Y.S., Ran, J.C., Chen, H.M., 2000. The characteristics of karst caves development in Libo, Guizhou. Carsol. Sin./Zhong Guo Yan Rong 19, 13–20.
Zhao, L.X., Zhang, L.Z., 2013. New fossil evidence and diet analysis of *Gigantopithecus blacki* and its distribution and extinction in South China. Quat. Int. 286, 69–74.
Zhao, Z.J., Liu, Y., Chen, Y., Zhang, M.H., Shu, Q., Li, C.L., 2013. Quaternary fluvial incision rates of the western Sichuan Plateau inferred from ESR chronology. J. Lanzhou Univ. 49, 160–165.
Zhao, Z.J., Granger, D.E., Zhang, M.H., Kong, X.G., Yang, S.L., Chen, Y., Hu, E.Y., 2016. A test of the isochron burial dating method on fluvial gravels within the Pulu volcanic sequence, West Kunlun Mountains, China. Quat. Geochronol. 34, 75–80.
Zhou, D.Q., Liu, X.M., Jiang, L.J., Liu, C.R., 2005. Step-like landforms and uplift of Guizhou Plateau. Earth Environ. 33, 79–84.
Zhu, S., 2012. River Landform and Geology Environment Evolution in the Yarlung Zangbo River Valley, (Doctoral Dissertation). Chinese Academy of Geological Science, Beijing.